Effect of humidity on friction, wear, and plastic deformation during nanoscratch of soda lime silica glass

Hongtu He,[1,2*] Qian Qiao,[1] Tongjin Xiao, [1] Jiaxin Yu,[1] and Seong H. Kim[2*]

[1] Key Laboratory of Testing Technology for Manufacturing Process, Ministry of Education, Southwest University of Science and Technology, Mianyang 621010, Sichuan, China

[2] Department of Chemical Engineering and Materials Research Institute, Pennsylvania State University, PA 16802, United States

*Corresponding address: hehongtu@swust.edu.cn (H. He), shk10@psu.edu (S.H. Kim)

Abstract: Physical flaws and defects on glass surfaces are known to reduce the mechanical strength and chemical durability of glass. The formation of surface defects depends on not only the mechanical conditions of the physical contact, but also the environment in which the contact is made. In this study, the nanoscratch behavior of soda lime silica (SLS) glass was investigated in 10% and 60% relative humidity (RH) conditions. Based on the evolution of friction and scratch depth, the deformation of SLS glass surface could be divided into four regimes: elastic deformation and recovery (E), RH-independent mild plastic deformation (P-1), RH-dependent intermediate plastic deformation (P-2), and RH-independent severe plastic formation (P-3). It is quite surprising to observe that plastic deformation of glass surface has a dependence on RH of the environment (outside the glass) because plastic deformation is the process occurring below the surface (inside the glass) by the externally applied load. From this result, it can be inferred that frictional energy dissipation mode at the sliding interface, which is a function of adsorbed water molecules, influences the subsurface deformation mode. Although friction, wear, and subsurface deformation/damage are all coupled, there is no direct one-on-one correlation among them.

Keywords: Soda lime silica glass; nanoscratch; deformation; elastic; plastic; humidity

1. Introduction

Silicate glasses are widely used in commercial products such as windows, containers, optics, etc. [1] and their applications are being extended to medical, energy, and environmental fields. [2-4] In applications under extreme conditions, however, the brittleness of silicate glasses poses technical challenges or practical limitations. [5] Such limitations are often related to the reduction of usable strength of glass due to the presence of surface defects and flaws generated by physical contacts with foreign objects. [6,7] Therefore, fundamental understanding of surface damage modes is crucial for controlling or preventing strength-limiting surface defects and flaws on glass objects.

Depending on the applied load during indentation or scratch, the deformation mode of solid materials can be generally divided into elastic, plastic, and cracking regimes. [8-11] For soda lime silicate (SLS) glass, distinct regimes of surface damage mode were observed in sequence of elastic, plastic, micro-cracking, chipping, and micro-abrasion upon increasing the applied normal load during the scratch test with a Vickers indenter tip. [12] Similar load-dependent surface damage modes can be found for silica glass when scratched with a Berkovich indenter tip with a normal load up to 300 mN. [13] When the surface of silica-based glass (such as fused silica and SLS) is scratched with a much sharper cono-spherical indenter tip, chipping can readily occur, with an apparent friction coefficient much higher than that in the elastic and plastic regimes. [14,15]

Apart from the applied load, the environmental conditions, such as the presence of water vapor, are known to alter the surface chemistry of silicate glass. Without a physical contact, water molecules can react with silicate glass surface via diffusion and hydration as well as hydrolysis of Si-O-Si network, [16,17] and these chemical reactions can finally alter the glass topography,[18] network connectivity, [19] and nanomechanical properties.[20] With the physical

contact via indentation or scratch tests, water molecules adsorbed on glass surface in humid air can also alter the surface damage modes. For instance, the contact-induced cracking is known to be easier to propagate in high relative humidity (RH) conditions; under the same mechanical load, more scratch-induced cracking can be found on silica glass and SLS glass surfaces in high RH conditions, compared to the lower RH. [12] This is because the water molecules adsorbed from the gas phase can facilitate the hydrolysis of the Si-O-Si glass network at the crack tip under the influence of applied stress, which could be related to the classic stress-corrosion theory. [21] In reciprocating ball-on-flat friction tests with an applied normal stress (<400 MPa) much smaller than the indentation damage threshold, the material removal (wear) volume of oxide glasses is also found to be sensitive to the RH level of the environment. The wear volume of most silicate and borosilicate glasses increases with RH; [22-24] in contrast, the wear volume of SLS glass decreases as RH increases above 75-80%. More interestingly, the superior wear-resistance of SLS glass at high RH conditions can be enhanced or deteriorated by altering the Na^+ ions concentration in the subsurface region thermal poling or hydrothermal treatment. [25,26] These studies [22,26-29] collectively suggest that the peculiar wear resistance of SLS glass at high RH conditions is related to the leachable Na^+ ions as well as chemical interactions with adsorbed waters.

This paper investigates whether the material damage behavior under nano-scratch conditions is sensitive to the RH or not, which has not been studied systematically compared to the RH dependence of micro-cracking and mechanochemical wear behaviors of glass. The nanoscratch tests of SLS glass surface were performed with a sharp diamond indenter (relatively sharper than the sphere surface in the friction test; typically, a μm-scale diameter with <10 nm room-mean-square roughness) at the elastic and plastic deformation regimes, and the effect of

RH on the deformation, friction, and wear behavior of SLS glass were studied. The scratch (penetration) depth, residual depth, friction force during nanoscratch and surface damage after nanoscratch tests were quantitatively compared. The RH dependence of plastic deformation of SLS glass, which was surprising to observe, and possible mechanisms are discussed in this paper.

2. Experimental details

The air side of SLS float-glass panels with a thickness of 1 mm (AGC Inc., Tokyo, Japan) was used for this test. A 60° cono-spherical diamond tip with an effective radius of ~2 μm was used as a counter-surface for the nanoscratch tests, as shown in Fig. 1a. Prior to nanoscratch tests, SLS glass substrates were cleaned by rinsing with liquid ethanol and water followed by blow-drying with dry nitrogen gas. More details of the cleaning of glass substrates prior to nanoscratch tests can be found in our previous publications. [23,30,31]

The nanoscratch tests of SLS glass were carried out using an Agilent G200 nanoscratch system (Santa Clara, CA) at room temperature (~22 ℃) in 10% and 60% RH conditions. The RH in the chamber was controlled by flowing a gas stream mixed with pre-set ratios of dry air and water vapor. The RH around the sample was monitored with a hygrometer. The RH fluctuation was controlled within 3% from the target RH during the entire nanoscratch tests. The nanoscratch tests were conducted by linearly increasing the normal load from 0 mN to maximum scratch load (e.g. 10 mN, 15 mN, and 20 mN) across the lateral displacement of 50 μm. As shown in Fig. 1b, each nanoscratch experiment procedure was composed of three steps. Firstly, a pre-scan with a constant normal load of 10 μN was performed to get the initial glass surface morphology. Then, the tip moved back to the initial position and began to scratch the glass

surface under a given scratch load and speed condition, then the friction force and penetration (scratch) depth during nanoscratch were recorded simultaneously. The scratch speed varied from 0.5 to 5 μm/s. Finally, a post-scratch scan was carried out with the same tip at a normal load of 10 μN to get the residual depth profile of the nanoscratch along the scratch direction. To prevent possible artifacts of the deformed zone induced by adjacent nanoscratches, every scratch test was conducted with at least ~30 μm separation distance. Total four scratch tests were performed at each testing condition to ensure the repeatability of the experiments, and only representative data were shown in this paper. In addition, the surface damages of SLS glass were analyzed with scanning electron microscopy (SEM, EVO18, Zeiss, Germany).

3. Results and discussion

3.1 Effect of RH on nanoscratch-induced deformation of SLS glass

Fig. 2 compares the scratch (indentation) depth during the nanoscratch test while ramping the applied load at a constant rate in 10% and 60% RH conditions and the residual depth after the test. At the applied normal load below 10 mN, the indentation depth increases (up to 126±1 nm at 10 mN) but the residual depth of the nanoscratch region remains the same as the pristine glass surface. This implies the glass deformation is completely reversible, i.e., elastic, in this low load regime. As the normal load increases to 15 mN, the maximum scratch depth increases to 257±2 nm, and the maximum residual depth is 90±2 nm. The distinction between the purely elastic deformation below the 10 mN load and the occurrence of plastic deformation at 10-15 mN can be further verified by the surface damages via SEM images, as shown in Fig. S1 in Supporting Information. Note that no difference in penetration depth and residual depth in 10% and 60% RH conditions is observed at the load below 15 mN (Fig. 2).

With the further increase of the normal load from 15 mN to 20 mN, the scratch depth and residual depth continues to increase, and the humidity effect becomes prominent, as displayed in Fig. 2. In 10% RH, the maximum scratch depth and residual depth of the nanoscratch are 477±4 nm and 294±2 nm, respectively, by the time the applied load increases to 20 mN. They decrease to 381±3 nm and 195±2 nm, respectively, in 60% RH. This humidity effect does not seem to be a function of the sliding speed in the range from 0.5 to 5 μm/s (Fig. S2 in Supporting Information).

The effect of humidity on the residual depth of nanoscratch of the SLS glass surface could be explained with the difference in mechanochemical reactions at the sliding interface. It was found, from reactive molecular dynamics (MD) simulations, that there are substantial shear strains in the subsurface region upon frictional sliding in the dry condition and such strains are greatly reduced in humid conditions. [29] This difference was attributed to the formation of interfacial bridge bonds which could be suppressed in the presence of interfacial water. [29] Although the previous MD simulations were for a sodium silicate glass, a similar trend is expected for the SLS surface. It is known that the about 10% of the surface carbon atoms of the diamond surface are oxidized. [32,33] Although the diamond surface with such a low degree of surface oxidation would be much less reactive than the silica surface in terms of interfacial bridge bond formation in tribochemical reaction conditions, [34] similar reactions could still occur. In fact, the oxidation state of the diamond surface is known to affect the interfacial adhesion. [35] Unfortunately, the current study cannot provide any information how efficiently and quantitatively such interfacial bond formation reactions can occur at the diamond/glass interface during the nanoscratch. Nonetheless, our experimental data imply that the probability of forming chemical bonds between the oxidized functional groups of the diamond tip surface and the SLS glass surface is suppressed upon the adsorption of water molecules on the glass surface.

Therefore, in a relatively dry condition (10% RH), interfacial friction may induce a large degree of subsurface strain, thus it may lead to a deeper penetration depth and the correspondingly larger residual depth (Fig. 2). In contrast, when nanoscratch tests are performed in a relatively humid condition (60% RH), the subsurface strain will be significantly lower due to the presence of water molecules adsorbed at the sliding interface, resulting in lower probabilities of bond dissociation of glass substrate during friction and thus smaller plastic deformation.

3.2 Effect of RH on friction of SLS glass during scratching

The friction forces recorded as a function of normal load in 10% RH and 60% RH environments are compared in Fig. 3. The coefficient of friction (COF, μ) is defined as the slope of the linear regression between friction force and normal load, i.e., $\mu = \Delta F_f / \Delta F_N$. Based on the magnitude of μ, four regimes of the nanoscratch can be identified in Fig. 3: elastic deformation regime (E), and three plastic deformation regimes which are marked as P-1, P-2, and P-3, respectively, in Fig. 3.

In the elastic deformation (E), the friction force is initially below the detection limit of the lateral force sensor (when the normal load is ≤5 mN) and then gradually increases as the normal load further increases from 5 mN to ~11 mN; in this regime, the slope (=COF) is 0.12. It is noted that typical COF values measured for boundary lubrications are around 0.15 in the absence of plastic deformations and wear of the substrate, regardless of the substrate materials. [36] When the ethanol vapor was used to lubricant SLS glass/Pyrex glass interface, a COF of ~0.2 was obtained, along with ~5 nm depth subsurface damage which was revealed through a hydrothermal treatment. [26] Thus, the COF of 0.12 in the E regime could be interpreted as the

boundary lubrication effect of adsorbed (adventitious) molecules on the SLS glass surface. [37] Note that some subsurface damage in the silicate network may occur near the transition from E to P-1, [38] but its contribution to friction might be negligible, so the topography of the outmost surface remains unchanged.

In the P-1 regime (between 11 mN and 15 mN of the applied normal load), the plastic deformation begins to become prominent in the topography profile (Fig. 2), and the friction force increases with the normal load with a corresponding COF of ~0.5. As shown in Fig. 2, the tip penetration rate (= slope in the indentation depth vs. load plot) suddenly increases upon the transition from the E regime (with a COF of 0.12) to the P-1 regime (with a COF of 0.5). In Fig. 2, the tip penetration rate in 10% RH (~30 nm/nN) is slightly larger than that in 60% RH (~24 nm/nN) in the P-1 regime. This must be due to the difference in the interfacial bond formation and transfer of shear stress into the subsurface region. [29] The different penetration rate means that the rate of increase in contact area between the tip and the substrate is different (Fig. 2); however, the COFs does not seem to be sensitive to such a minute difference (Fig. 3). This implies that the COF does not solely depend on the total contact area. [39] As discussed earlier, [29] there are larger subsurface damages expected in 10% RH than 60% RH; thus, the resistance to tip sliding (shear stress) might be lower for the subsurface region damaged in 10% RH, thus the overall friction might be similar to the 60% case even though the total contact area might be slightly larger in 10% RH. [40]

When the applied normal load increases above 15 mN, the COF abruptly increases from the value of the P-1 regime and there is a large difference between two RH conditions as the load increases up to ~18 mN. Above the 18 mN, the COF ($=\Delta F_f / \Delta F_N$) becomes similar again. Hereafter, the 15-18 mN region is called the P-2 regime and the region above 18 mN is called the

P-3 regime. In 10% RH, the transition from P-1 to P-2 coincides with the change in the tip penetration rate from ~30 nm/nN to ~39 nm/nN (Fig. 2); in 60% RH, however, this transition in COF occurs without any noticeable change in the tip penetration rate (~26 nm/nN in Fig. 2). The tip penetration rate is significantly higher in 10% RH, as compared to 60% RH, due to more severe subsurface damage as indicated from reactive MD simulations. [29] Unlike the P-1 regime, it appears that the faster increase in the tip-surface contact area upon increasing the load becomes a dominant factor determining the magnitude of COF.

In the P-3 regime, the COFs ($=\Delta F_f/\Delta F_N$) at 10% and 60% RH becomes similar to each other, although their actual friction forces are different. Interestingly, the tip penetration rates also become similar in the 18-20 mN region in Fig. 2, although their actual penetration depths are different. It is somewhat surprising that the COF values at different RHs are close to each other because the penetration depth (which determines the contact area and the degree of subsurface deformation) as well as the magnitude of friction force are all different in this regime.

Similar to the COF, the plastic deformation of nanoscratch can also be divided into three regimes according to the evolution of plastic fraction of nanoscratch (Fig. 4). The plastic fraction is defined as the ratio of the residual depth after the scratch to the penetration depth during the scratch. Obviously, this fraction is zero in the E regime. In the P-1 regime, the plastic fraction increases with normal load at the almost identical rate in 10% and 60% RH conditions, which is similar to the COF change in this regime (Fig. 3). Reflecting the higher tip penetration rate in 10% RH, the plastic fraction in the P-2 regime is higher in 10% RH. Because more plastic deformation occurs in 10% RH, more energy must have consumed than 60% RH, thus it will contribute to a larger increase in friction (thus, higher COF) in 10% RH. [41]

This RH-dependence of plastic fraction in the P-2 regime is quite surprising. One may question whether water molecules ingress into the glass faster during the plastic deformation in higher RH conditions. If that happened, then those water molecules could have facilitated the Si-O-Si hydrolysis, according to the stress corrosion theory, [21] and prevented the reformation of the Si-O-Si bridging bonds of the network. [29] Then, the penetration depth would have been larger and the plastic fraction would have been larger in higher RH conditions. However, this is opposite to the experimental observations (Fig. 2 and 4). Thus, it is unlikely that the water molecules impinging from the gas phase will ingress into the glass (underneath or near the nanoscratch tip) *during* the plastic deformation in the P-2 regime, although it cannot be ruled out the possibility of more water ingress into the damaged subsurface region in high RH condition *after* the nanoscratch tip is removed.

If the water ingress into the subsurface region during the plastic deformation is negligible, the RH-dependence of plastic fraction in the P-2 regime could be related to the water-induced tribochemical reactions at the shear plane between the tip and glass surface. In low RH, the subsurface damages underneath the nanoscratch will be larger because more mechanical energy can be transferred to the subsurface, accompanying with more severe disruptions of the silicate network bond.[29] Consequently, deeper scratch depth (Fig. 2) and less elastic recovery (lager plastic fraction in Fig. 4) can occur in low RH. In high RH, more tribochemical reactions involving interfacial water molecules take place readily at the sliding interfaces, consuming more frictional energy at the interface and thus transferring less energy into the subsurface region;[29] this may result in less scratch depth and more elastic recovery (less plastic fraction) in high RH (Fig. 2 and 4).

In the P-3 regime, the plastic fractions at two different RH conditions converge to the same value, ~65% (Fig. 4). In this regime, the tip penetration rate (Fig. 2) and the COF (Fig. 3) are also similar in these two RH conditions. This might mean that the nanoscratch-induced mechanical damage is so severe at this regime that the difference in mechanochemistry at the sliding interface is not significant.

3.3 Effect of RH on wear pattern of SLS glass during scratching

In addition to the physical deformation into the substrate (Fig. 2) and the COF (Fig. 3), the wear mode of SLS glass upon nanoscratch evolves differently depending on the applied load and the humidity of the test condition, as shown in Fig. 5. The different regimes identified in Figs. 2-4 are marked in the low magnification images, based on the distance from the end point of the nanoscratch test. Obviously, there is no visible damage in the E regime. In the P-1 regime, although the penetration depth, COF, and plastic fraction are very similar for 10% and 60% RH (Fig. 2-4), the wear pattern observed in SEM is quite distinct. In the case of nanoscratch tracks produced in 10% RH (Fig. 5a), the track does not have clearly-identifiable wear pattern at the beginning of the P-1 regime and pile-ups can be seen in the region before the P-2 regime starts. In the case of the track produced in 60% RH (Fig. 5b), wear debris can be seen right after the transition from E to P-1. One complication here is that the SEM image in Figure 5 shows that the pile-up shape looks quite different from that of shear flow of pure bulk materials (such as in the case of tensile metals) due to the brittleness of glass and the mechanochemical wear in the presence of water vapor in the environment. If this complication is ignored and we use the fact that the densification and shear flow are a hydrostatic (volume-changing, but shape-conservative) and deviatoric (volume-conservative, but shape-changing) process, respectively, then the relative

densification ratio of glass can be roughly estimated by the relative ratio between the pile-up height and residual depth of nanoscratch mark. In the P-1 regime, although the penetration depth, COF, and plastic fraction are very similar for two RH environments, the pile-up in 60% RH is more obvious than that in 10% RH. The same residual depth (lateral displacement 40-52 μm region in Figure 2) and higher pile-up formation (Figure 5b) in 60% RH implies that in the P-1 regime, the nanoscratch-induced subsurface densification of SLS glass must lower in 60% compared to 10% RH.

It is interesting to note that the shape of wear debris extruded from the nanoscratch track is quite different depending on the RH of the environment: 10% vs. 60% RH. The wear debris produced in 10% RH look more like micro-cracks of extrudates.[39] As the applied load increases in the P-2 and P-3 regime, there are more particles produced due to such cracking or chipping. In contrast, the periodic break patterns in the wear debris produced in 60% RH look like 'melt fracture' or 'sharkskin' of extrudates; [42] this wear debris pattern could be attributed to the tribochemical reaction products formed at the shear plane in high humidity conditions, [43] which may be squeezed out as a partially-wet paste that undergoes simultaneous drying. In the P-2 regime, the penetration depth, residual depth, COF, and plastic fraction in 60% RH are smaller than those in 10% RH, but the height of wear debris and pile-up appear to be similar or slightly larger based on the image contrast in SEM. These observations suggest that the subsurface densification in the P-2 regime is still lower in 60% RH as compared to the 10% RH due to the lower frictional energy dissipated at the sliding interface and transferred into subsurface. In the P-3 regime, the subsurface densification of SLS glass in 60% RH could also be lower than that in 10% RH based on the final topography between the pile-up height and residual depth. Thus, the experimental data presented in this study, combined with the previous study, [29] indicate the

adsorbed water molecules on glass surfaces can mitigate the surface damage and subsurface deformation of SLS glass during nanoscratch. More quantitative study requires sub-T_g annealing and subsequent characterizations, which will be the subject of a future study.

Generally, the friction and wear behaviors of solid materials depend on not only the mechanical contact conditions, but also the surface chemical composition, microstructures, and the test environment. [44-46] The difference in the frictional energy dissipation mode at the shear plane will have a huge impact on the subsurface damage pattern. [47,48] As a result, the relationship among the friction, wear, and subsurface damage may vary in very complicated ways. For instance, one may find a higher COF along with lower wear rate of amorphous carbon film and ceramic surfaces in vacuum, [49] or high wear volume but low subsurface damage of phosphate glass in liquid water. [50] Overall, the data presented here reveal that although the friction, wear, and subsurface deformation/damage of solid materials are all coupled, there is no direct one-on-one correlation among them.

4. Conclusions

The effects of humidity on the friction, wear, and plastic deformation of SLS glass surface during nanoscratch were investigated in the present study. Based on the evolution of COF and plastic deformation fraction, the nanoscratch on SLS glass surface can be divided into an elastic regime and mild, intermediate, and severe plastic deformation regimes. The plastic deformation of SLS glass surface shows the RH dependence behavior to some extent, which can be attributed to changes in interfacial friction and mechanochemical reactions at the sliding interface with the environmental RH. These findings indicate that although the friction, wear,

and subsurface deformation/damage of solid materials are all coupled, the direct one-on-one correlation among them may not be found.

Acknowledgements. The authors are grateful for the financial support from the National Natural Science Foundation of China (Grant No. 51605401), Scientific Research Fund of SiChuan Provincial Education Department (17ZA0408), and Natural Science Foundation of United States of America (Grant No. DMR-2011410). HH is also grateful for the funding from Southwest University of Science and Technology (18LZX515).

References

1. Axinte E. Glasses as engineering materials: A review. Mater Des. 2011;32:1717-1732.
2. Ramanujam J, Singh UP. Copper indium gallium selenide based solar cells-a review. Energy Environ Sci. 2017;10:1306-1319.
3. Kansal I, Goel A, Tulyaganov DU, Santosd LF, Ferreira JMF. Structure, surface reactivity and physico-chemical degradation of fluoride containing phospho-silicate glasses. J Mater Chem. 2011;21:8074-8084.
4. Luo W, Khoo YS, Hacke P, Naumann V, Lausch D, Harvey SP, Singh JP, Chai J, Wang Y, Aberle AG, Ramakrishna S. Potential-induced degradation in photovoltaic modules: a critical review. Energy Environ Sci. 2011;10: 43-68.
5. Wondraczek L. Overcoming glass brittleness. Science . 2019;366(6467):804-805.
6. Varshneya AK. Stronger glass products: Lessons learned and yet to be learned. Int J Appl Glass Sci. 2018;9(2):140-155.

7. Benzine O, Bruns S, Z, Pan, Durst K, Wondraczek L. Local deformation of glasses is mediated by rigidity fluctuation on nanometer scale. Adv Sci. 2018;5:1800916.

8. Armstrong RW, Elban WL, Walley SM. Elastic, plastic, cracking aspects of the hardness of materials. Int. J. Mod. Phys. B. 2013;27(8):1330004. 1

9. Xu N, Han W, Wang Y, Li J, Shan Z. Nanoscratching of copper surface by CeO_2. Acta Mater. 2017;124:343-350.

10. de Voorde BV, Ameloot R, Stassen I, Everaert M, Vos DD, Tan J. Mechanical properties of electrochemically synthesised metal-organic framework thin films. J Mater Chem C. 2013;1 :7716-7724.

11. Ye YX, Liu CZ, Wang H, Nieh TG. Friction and wear behavior of a single-phase equiatomic TiZrHfNb high-entropy alloy studied using a nanoscratch technique. Acta Mater. 2018;147 :78-89.

12. Le Houerou V, Sangleboeuf JC, Dériano S, Rouxel T, Duisit G. Surface damage of soda-lime-silica glasses: indentation scratch behavior. J Non-Cryst Solids. 2003;316 (1):54-63.

13. Moayedi E, Wondraczek L. Quantitative analysis of scratch-induced microabrasion on silica glass. J. Non-Cryst Solids. 2017;470:138-144.

14. Lee K, Marimuthu KP, Kim C, Lee H. Scratch-tip-size effect and change of friction coefficient in nano / micro scratch tests using XFEM. Tribol Int. 2018;120:398-410.

15. Sawamura S, Limbach R, Wilhelmy S, Koike A, Wondraczek L. Scratch-induced yielding and ductile fracture in silicate glasses probed by nanoindentation. J Am Ceram Soc. 2019;102:7299-7311.

16. Schnatter KH, Doremus RH, Lanford WA. Hydrogen analysis of soda-lime silicate glass. J Non-Cryst Solids 1998;102(1-3):11-18.

17. Gy R. Stress corrosion of silicate glass: a review. J Non-Cryst Solids 2003;316(1): 1-11.

18. Ngo D, Liu H, Kaya H, Chen Z, Kim SH. Dissolution of silica component of glass network at early stage of corrosion in initially silica-saturated solution. J Am Ceram Soc 2019;102(11): 6649-6657.

19. Kaya H, Ngo D, Gin S, Kim SH. Spectral changes in Si-O-Si stretching band of porous glass network upon ingress of water. J Non-Cryst Solids 2020;527:119722.

20. Kolluru PV, Green DJ, Pantano CG, Muhlstein CL. Effects of surface chemistry on the nanomechanical properties of commercial float glass. J Am Ceram Soc. 2010;93(3):838- 847.

21. Ciccotti M. Stress-corrosion mechanisms in silicate glasses. J Phys D Appl Phys. 2009;42:214006.

22. Bradley LC, Dilworth ZR, Barnette AL, Hsiao E, Barthel AJ, Pantano CG, Kim SH. Hydronium ions in soda-lime silicate glass surfaces. J Am Ceram Soc. 2013;96:458-463.

23. He H, Qian L, Pantano CG, Kim SH. Mechanochemical wear of soda lime silica glass in humid environments. J Am Ceram Soc. 2014;97(7): 2061-2068.

24. Surdyka ND, Pantano CG, Kim SH. Environmental effects on initiation and propagation of surface defects on silicate glasses: Scratch and fracture toughness study. Appl Phys A. 2014;116:519-528.

25. He H, Luo J, Qian L, Pantano CG, Kim SH. Thermal Poling of soda-lime silica glass with nonblocking electrodes-Part 2: Effects on mechanical and mechanochemical properties. J Am Ceram Soc. 2016;99:1231-1238.

26. Luo J, Huynh H, Pantano CG, Kim SH. Hydrothermal reactions of soda lime silica glass-revealing subsurface damage and alteration of mechanical properties and chemical structure of glass surfaces, J Non-Cryst Solids. 2016;452:93-101.

27. Luo J, Banerjee J, Pantano CG, Kim SH. Vibrational sum frequency generation spectroscopy study of hydrous species in soda lime silica float glass. Langmuir. 2016;32: 6035-6045.

28. Sheth N, Luo J, Banerjee J, Pantano CG, Kim SH. Characterization of surface structures of dealkalized soda lime silica glass using x-ray photoelectron, specular reflection infrared, attenuated total reflection infrared and sum frequency generation spectroscopies. J Non-Cryst Solids. 2017; 474:24-31.

29. Hahn SH, Liu H, Kim SH, van Duin ACT. Atomistic understanding of surface wear process of sodium silicate glass in dry versus humid environments. J Am Ceram Soc. 2020;103:3060-3069.

30. Barthel AJ, Luo J, Hwang KS, Lee JY, Kim SH. Boundary lubrication effect of organic residue left on surface after evaporation of organic cleaning solvent. Wear. 2016;350-351:21-26.

31. Qiao Q, He H, Yu J. Evolution of HF etching rate of borosilicate glass by friction-induced damages. Appl Sur Sci. 2020;512:144789.

32. Petrini D, Larsson K. Theoretical study of the thermodynamic and kinetic aspects of terminated (111) diamond surfaces. J Phys Chem C. 2008;112(8): 3018-3026.

33. Shergold HL, Hartley CJ. The surface chemistry of diamond. Int J Mineral Process. 1982;9(3):219-233.

34. He H, Kim SH, Qian L. Effects of contact pressure, counter-surface and humidity on wear of soda-lime-silica glass at nanoscale. Tribol Int. 2016;94:675-681.

35. Sumant AV, Grierson DS, Gerbi JE, Carlisle JA, Auciello O, Carpick RW. Surface chemistry and bonding configuration of ultrananocrystalline diamond surfaces and their effects on nanotribological properties. Phys Rev B. 2007;76:235429.

36. Barthel AJ, Kim SH. Lubrication by physisorbed molecules in equilibrium with vapor at ambient condition: Effects of molecular structure and substrate chemistry. Langmuir. 2014;30: 6469-6478.

37. Lin Y, Smith N, Banerjee J, Agnello G, Manley RG, Walczak WJ, Kim SH. Water adsorption isotherm on silica and calcium-boroaluminosilicate glass surfaces-Thickness and hydrogen bonding of water layer. J Am Ceram Soc. 2021;104(3): 1568-1580.

38. He H, Chen Z, Lin Y, Hahn SH, Yu J, van Duin ACT, Gokus TD, Kim SH. Subsurface structural change of silica upon nanoscale physical contact: Chemical plasticity beyond topographic elasticity. Acta Mater. 2021;208:116694.

39. Bensaid N, Benbahouche S, Roumili F, Sangleboeuf JC, LeCam JB, Rouxel T. Influence of the normal load of scratching on cracking and mechanical strength of soda-lime-silica glass. J Non-Cryst. Solids .2018;483:65-69.

40. Mo Y, Turner K, Szlufarska I. Friction laws at the nanoscale. Nature. 2009;457:1116-1119.

41. Pietrement O, Troyon M. Study of the interfacial shear strength pressure dependence by modulated lateral force microscopy. Langmuir. 2001;17:6540-6546.

42. Kulikov O, Hornung K, Wagner M. Silanols cured by borates as lubricants in extrusion of LLDPE. Impact of elasticity of the lubricant on sliding friction. Rheol Acta. 2007;46:741-754.

43. Chen L, Wen J, Zhang P, Yu B, Chen C, Ma T, Lu X, Kim SH, Qian L. Nanomanufacturing of silicon surface with a single atomic layer precision via mechanochemical reactions. Nat Commun. 2018;9(1):1542.

44. Guo Y, Zhang L, Zhang G, Wang D, Wang T, Wang Q. High lubricity and electrical responsiveness of solvent-free ionic SiO_2 nanofluids. J Mater Chem A. 2018;6:2817-2827.

45. Chen Z, He X, Xiao C, Kim SH. Effect of humidity on friction and wear: A critical review. Lubricants. 2018;6(3):74.

46. Liu X, Pu J, Wang L, Xue Q. Novel DLC/ionic liquid/graphene nanocomposite coatings towards high-vacuum related space applications. J Mater Chem A. 2013;1:3797-3809.

47. Yeo RJ, Dwivedi N, Zhang L, Zhang Z, Lim CYH, Tripathy S, Bhatia CS. Superior wear resistance and low friction in hybrid ultrathin silicon nitride/carbon films: Synergy of the interfacial chemistry and carbon microstructure. Nanoscale. 2017;9:14937-14951.

48. Meshi L, Samuha S, Cohen SR, Laikhtman A, Moshkovich A, Perfilyev V, Lapsker I, Rapoport L. Dislocation structure and hardness of surface layers under friction of copper in different lubricant conditions. Acta Mater. 2011; 59: 342-348.

49.Zhang W, Tanaka A, Wazumi K, Koga Y. Effect of environment on friction and wear properties of diamond-like carbon film. Thin Solid Films. 2002; 413: 104-109.

50.Ye J, Yu J, He H, Zhang Y. Effect of water on wear of phosphate laser glass and BK7 glass, Wear. 2017; 376: 393-402.

List of figure captions

Fig. 1 (a) Schematic illustration of the nanoscratch test of SLS glass surface with a cono-spherical nanoindenter tip. The tip image here is cropped from an SEM image of the actual tip. (b) Load and lateral displacement functions used for the nanoscratch experiment.

Fig. 2 Penetration depth and residual depth of nanoscratch on SLS glass surface. The applied normal load is 10, 15, and 20 mN, respectively. The contact pressure is calculated based on the Hertz contact theory. The average contact pressure at 20 mN is 11.6 GPa when the RH is 10%.

Fig. 3 Friction force as a function of normal load for SLS glass surface in 10% RH and 60% RH environments. The error bar is the standard error of mean (SEM) from 4 measurements under the given conditions.

Fig. 4 Plastic fraction of nanoscratch on SLS glass surface as a function of applied load. The error bar is the standard error of mean (SEM) from 4 measurements under the given conditions.

Fig. 5 SEM images of nanoscratch of SLS glass in (a) RH=10% and (b) RH=60% environments. A nanoscratch with the same distance under the constant loading mode is made for comparison.

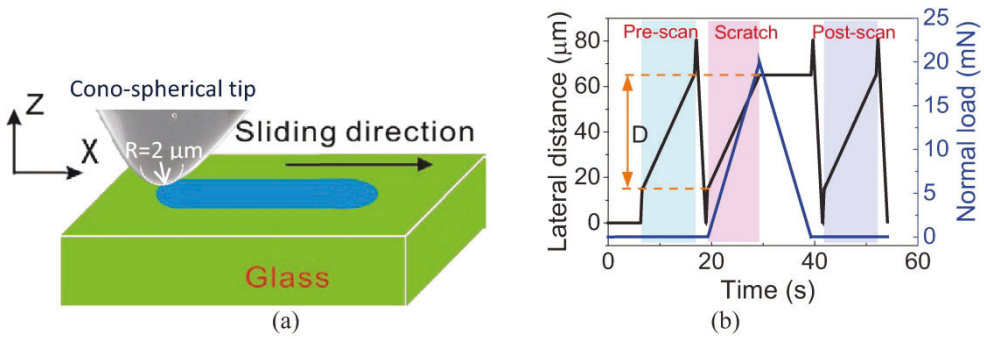

Fig. 1 (a) Schematic illustration of the nanoscratch test of SLS glass surface with a cono-spherical nanoindenter tip. The tip image here is cropped from an SEM image of the actual tip. (b) Load and lateral displacement functions used for the nanoscratch experiment.

167x63mm (600 x 600 DPI)

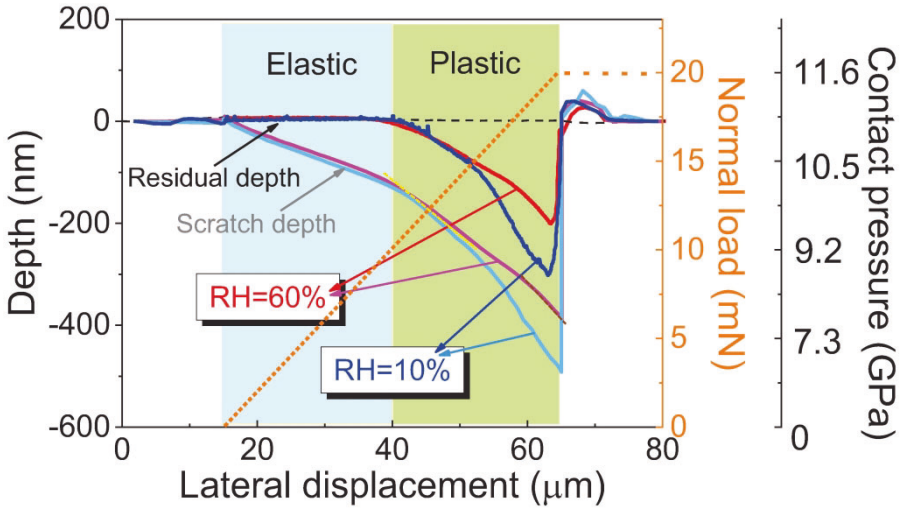

Fig. 2 Penetration depth and residual depth of nanoscratch on SLS glass surface. The applied normal load is 10, 15, and 20 mN, respectively. The contact pressure is calculated based on the Hertz contact theory. The average contact pressure at 20 mN is 11.6 GPa when the RH is 10%.

153x91mm (600 x 600 DPI)

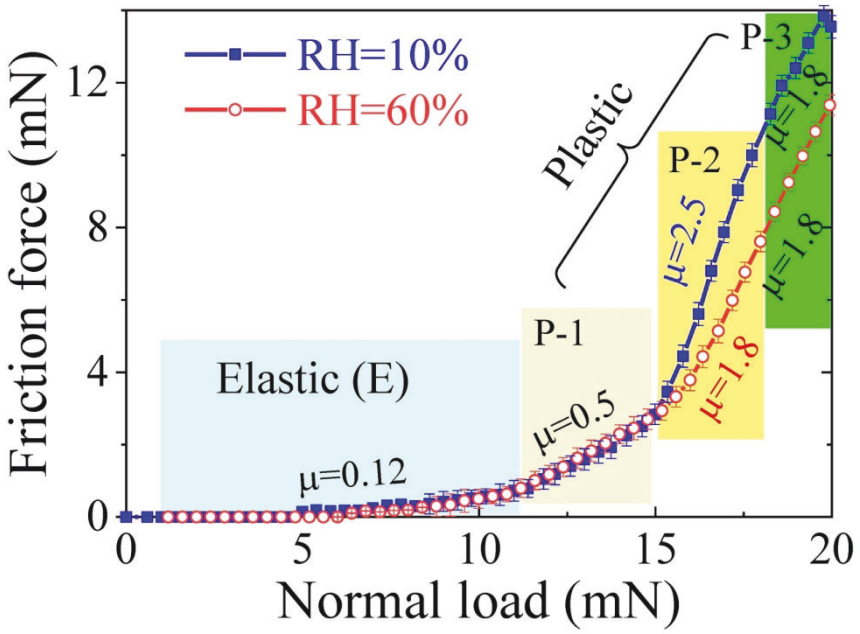

Fig. 3 Friction force as a function of normal load for SLS glass surface in 10% RH and 60% RH environments. The error bar is the standard error of mean (SEM) from 4 measurements under the given conditions.

128x90mm (300 x 300 DPI)

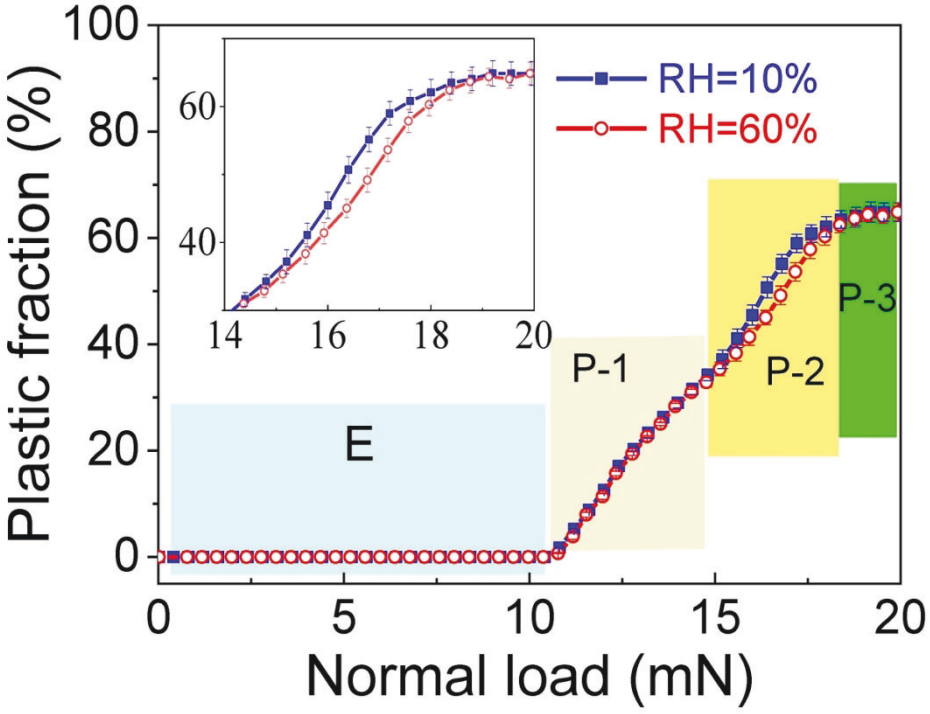

Fig. 4 Plastic fraction of nanoscratch on SLS glass surface as a function of applied load. The error bar is the standard error of mean (SEM) from 4 measurements under the given conditions.

113x84mm (300 x 300 DPI)

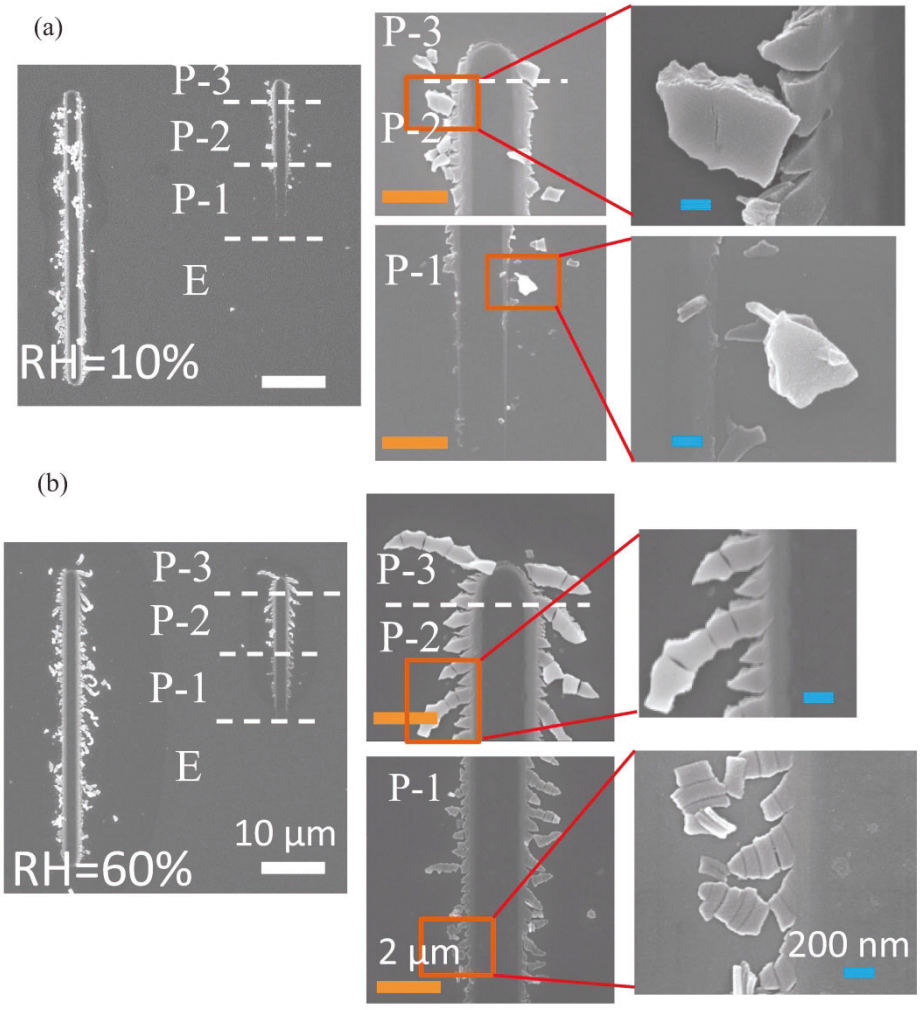

Fig. 5 SEM images of nanoscratch of SLS glass in (a) RH=10% and (b) RH=60% environments. A nanoscratch with the same distance under the constant loading mode is made for comparison.

157x166mm (600 x 600 DPI)

Effect of humidity on friction, wear, and plastic deformation during nanoscratch of soda lime silica glass

Hongtu He,[1,2*] Qian Qiao,[1] Tongjin Xiao, Jiaxin Yu,[1] and Seong H. Kim[2*]

[1] Key Laboratory of Testing Technology for Manufacturing Process, Ministry of Education, Southwest University of Science and Technology, Mianyang 621010, Sichuan, China

[2] Department of Chemical Engineering and Materials Research Institute, Pennsylvania State University, PA 16802, United States

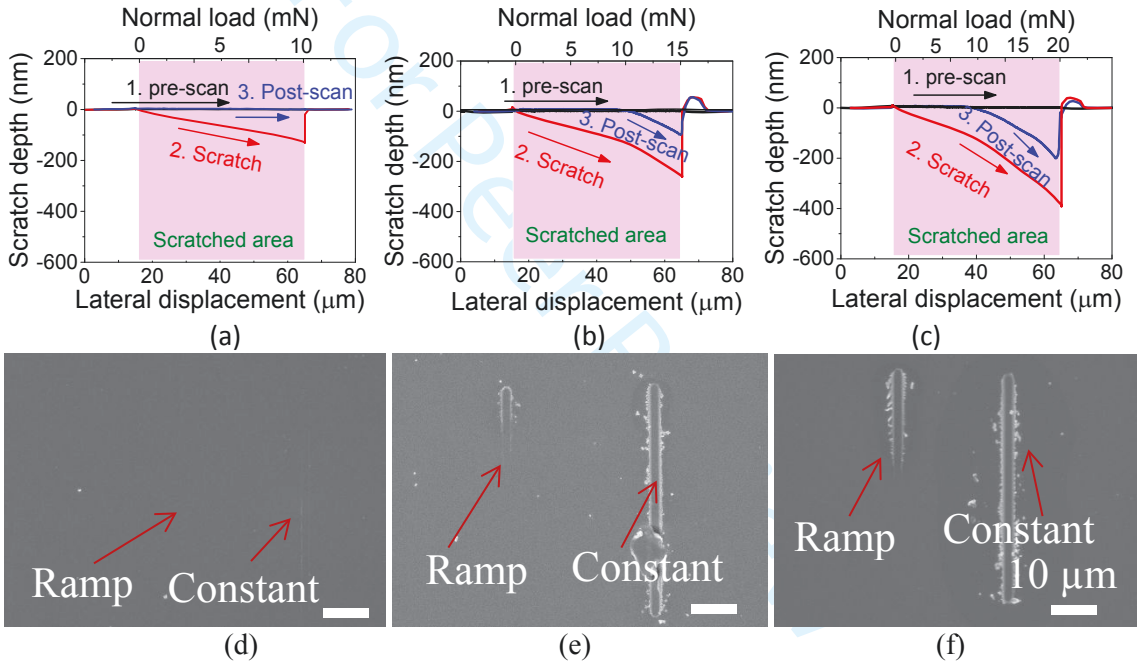

Fig. S1 Scratch depth as a function of lateral displacement under the ramp loading mode of (a) 10 mN, (b) 15 mN, and (c) 20 mN. The corresponding SEM images of scratch morphology of soda lime glass under a ramp loading mode of (d) 10 mN, (e) 15 mN, and (f) 20 mN. The scratch speed is 2 μm/s, and the environment humidity is 60% RH.

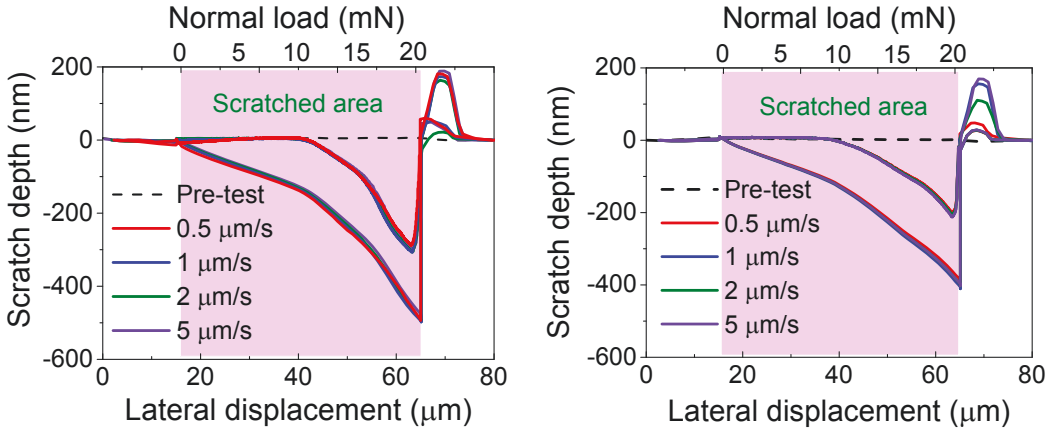

Fig. S2 Effects of scratching speed on the scratch depth as a function of lateral displacement of the ramp loading mode in (a) 10% RH and (b) 60% RH environments. The ramp load is 20 mN.